Temporal Evolution and Spatial Distribution of Dust Creation Events in Tore Supra and in ASDEX Upgrade Studied by CCD Image Analysis

Suk-Ho Hong[1,†], Christian Grisolia[2], Volker Rohde[3], Pascale Monier-Garbet[2], Tore Supra team[2], and ASDEX Upgrade team[3]

[1]*National Fusion Research Institute,*

113 Gwahangno, YuSung-Gu, DaeJeon, 305-333, Republic of Korea

[2]*Association EURATOM-CEA/Cadarache, DSM/IRFM,*

St. Paul les Durance, 13108, France

[3]*Max-Planck-Institut für Plasmaphysik, Association EURATOM-Association,*

85748 Garching, Germany

Abstract

Images of wide-angle visible standard CCD cameras contain information on Dust Creation Events (DCEs) that occur during plasma operations. Analyzing the straight line-like dust traces in shallow cylindrical shell-structured scrape-off layer along the vacuum vessel, caused by plasma-dust interaction, database on the DCEs are built. The database provides short/long term temporal evolution and spatial distribution of origins of DCEs in fusion devices. We have studied DCEs of CIMES (2006) and DITS (2007) Tore Supra (TS) campaigns, and DCEs of 2007 ASDEX Upgrade (AUG) campaign. The results from the TS CIMES campaign show different patterns of DCEs meaning different plasma-wall interaction depending on power coupling. TS DITS campaign indicates that dusts may be an operational limit if a fixed plasma operation scenario is used repeatedly. Different behaviours of DCEs between carbon limiter machine and full tungsten divertor machine are found, which is important for next generation fusion machine like ITER.

1. Introduction

Plasma-wall interaction causes both erosion of the plasma facing components (PFCs) and re-deposition on the PFCs. The net effect is determined by the local balance between erosion and re-deposition. Two major problems caused by re-deposited layer on the PFCs in machines using graphite are fuel retention and the creation of flakes and dusts. After the JET DTE1 campaign, it was estimated that about 10 % of injected tritium (35 g) was trapped in deposited a-C:H layers [1]. If the thickness of re-deposited layers exceeds a sustainable limit (depending on machines and layer condition [2]) due to

[†]sukhhong@nfri.re.kr

internal stress, the adhesion of the layer decreases, inducing flaking which is main source of mobilizable dusts in tokamaks [3]. The flaking process can be obviously increased by external constraints as thermal shock during ELMs or disruption.

In-vessel dusts will be one of critical issues for next generation fusion machine like ITER since they impact on safety and operation issues. In future fusion machine as ITER, dusts will be activated, tritiated and potentially chemically toxic (presence of beryllium) [4]. Several safety limits (as in-vessel dust total quantity) have been set in the frame of the ITER project in order to manage the potential dust hazards [5, 6]. As a consequence, it is mandatory to implement new dust diagnostic systems as well as tools that are able to recover and extract the micro-particles/flakes from the future tokamak vessel.

In order to control and monitor in-vessel dusts, the in-vessel spatial location from where dusts are created and to where dusts are transported must be identified. The temporal evolution of the DCEs is another important issue to be studied as well as how often DCEs occur during the plasma operation. Knowing the spatial distributions and the term temporal behaviours of the DCEs, strategies for the dust removal can be determined, when and how often the dust removal has to be performed: in-between pulses, daily bases, or after a campaign.

Local detection and dust density measurements by using laser light scattering are possible [7, 8]. Nevertheless, diagnostics based on “line-of-sight” measurements are not adequate for the research of global behaviour of in-vessel dusts, because the creation frequency of dusts is random and the trajectories are widely spread in the vacuum vessel. In order to locate the origin of the dust creation and to study the temporal behaviour of the dusts, CCD cameras installed in fusion devices are one of the best methods for the study of the global behaviour of dusts. Mobilized dusts, usually called “UFOs”, micro-particles entering the tokamak edge plasma are thermally heated resulting in thin visible trajectories observed easily in CCD camera movies just like meteors entering the earth atmosphere [9, 10, 11].

The aim of this paper is to demonstrate the possible use of standard visible CCD cameras installed in fusion devices as a dust diagnostic and to discuss the temporal evolution and the spatial distribution of DCEs observed by visible CCD cameras installed in the Tore Supra (TS) and in the ASDEX Upgrade (AUG). Visible CCD images are analyzed frame by frame by an image processing method developed in TS and described in detail elsewhere [12].

This paper is organized as follows. In section 2, the image processing method [12] will be briefly recalled. The results, short/long term temporal evolution and spatial distribution of DCEs in TS and in AUG campaigns are discussed in detail in section 3 and discussion is followed in section 4. Finally summary and conclusion are given.

2. Brief Description of Image Processing

In most cases, image processing is “pattern recognition” obtained by tracing specific target patterns of interests (called foreground) that show differences among “static objects” in sequential frames (called background). In the case of in-vessel dust research using visible CCD cameras, the target pattern is “well defined straight line-like trajectories of dusts” in shallow shell-structured volume of scrape-off layer along the surface of vacuum vessel that are present in the CCD images due to the interaction with the plasma. By analyzing these dust trajectories, statistics of the in-vessel DCEs are established.

2.1 General Remarks

We would like to give some general remarks on the idea of image processing for more clear understanding.

First, it is worth to mention when we can detect dusts at all. Major dust creation processes in tokamaks are flaking and arcing [2]: The adhesion of layer is getting poor and poor as thickness of deposit on PFC increases. This leads to the poor contact between layer and main part of PFCs, causes heating of the layers. In TS, for instance, the temperature of some layers (hot flakes) on the TPL during plasma operation is up to 1800 °C that emit thermally intensive light before they flake [13]. Thus, hot flakes ejected from the layers (including flaking during disruptions) are detected, of course, immediately after their ejection [13]. The intensity of light from dusts depends on their size, material density (composition), and temperature of dusts (>2500 K [14]). After they enter the scrape-off layer, dusts are heated further by interaction with edge plasma: Amount of light emitted depends on the strength of interaction with plasma. Similarly, arcing produces dusts and metal droplets. Arcing heats locally PFCs thus dusts produced by arcing are also heated. Thus, these make the dusts observable immediately after their ejection. A problem in this case is the saturation of pixels by intensive emission as described in our paper [12].

Note that, we cannot measure "size" of dusts by CCD cameras that have low spatial resolution than size of dusts. Detailed discussion on this topic is beyond the scope of this paper. An object smaller than spatial resolution of CCD camera (corresponding to a pixel) will be detected by a pixel regardless of their actual size: They show only intensity difference due to their different temperatures caused by different size, material composition, or the strength of interaction with plasma. Calculation shows that 1 μm carbon dust can survive more than 1 second in the plasma and dusts should have temperature more than 2500 K, because below this temperature the thermal evaporation is not triggered [14]. They also suggest that ~1 μm dusts of a few 1000 K will be seen directly by cameras [14]. Even μm size of arching events are detected by CCD cameras, although actual size of the arching spot is much smaller than the spatial resolution of a pixel, because they emit intensive light. The same fact holds for smaller dusts. If dusts are hot enough so that they emit enough photons, they will be detected by CCD cameras. Recent paper from DIII-D, detection limit of dust by fast CCD camera was 3 μm [15]. They have used DiMES system to inject pre-calibrated “cold” carbon dust particles. In this case, dusts need to be

heated by interaction with plasma before they become visible. Smaller particles would immediately disappear after their exposition to the plasma before they are detected by CCD camera due to their short lifetime compared with exposition time of CCD cameras.

Therefore the detection limit of dust by CCD cameras depends strongly not only on the size and spatial resolution of CCD cameras, but also temperature of dusts and material density. Some machines have reported small dust size distribution (DIII-D 0.3-0.9 μm, Alcator 0.3-1.1μm, TFTR 1.6-2.7 μm [16]), some other machines have reported larger dust size (Tore Supra 2.68±2.77 μm, LHD 3.0-14.39 μm, AUG 1.42-5.5 μm [16, 17]). Average sizes of TS and AUG dusts found after machine vent were over 3 μm, and they are sufficiently large that they survive much longer in plasmas and hot enough to be detected by CCD cameras during the plasma shot. Nevertheless, DIII-D value of 3 μm would be feasible as a lower observation limit of CCD camera. Note that, Thompson system detects many dusts (events) while CCD cameras do not record any event [8]. These dusts are under the detection limit of CCD camera and the discussion about the validity of modeling of these dusts by Rayleigh or Mie theory is beyond the scope of this paper, thus will not be discussed. Nevertheless, size distribution of dusts detected by CCD cameras during the plasma operation and collected during the maintenance may be different due to various dust creation mechanism (volume polymerization, brittle destruction, flaking, and arching) and due to plasma-dust interaction (erosion, mostly).

Second, exact location of a “flying object” in 3D cannot be extracted from 2D image in general. Depth information is lost during the conversion from 3D to 2D: Dust observation at any particular pixel can occur anywhere along the line of sight of that pixel. In such a case, it is impossible to determine exact location of dust trajectories in 3D space observed by the pixel (e.g., DCEs from the edge of HFS (label A in Figure 6) and LFS behind). Nevertheless, most of dust trajectories seen by visible CCD cameras are distributed in shallow volume of cylindrical shell-structured scrape-off layer (SOL) along the walls, so that they are relatively clearly distinguishable. In this paper, we do not mention or argue that we determine “exact spatial location of dusts” in 3D space or trace “individual trajectory”, but we determine statistically “*the most possible origin of DCEs*” by overlapping dust trajectories: There would exist statistical error. These are conditions with which origins of DCEs can be determined:

1. Dusts cannot penetrate into the core plasma.
2. Dusts are distributed in shallow volume of cylindrical shell-structured scrape-off layer along the surface of vacuum vessel compared with the thick core plasma.
3. The origins of DCEs are determined by statistical weighting by overlapping huge amount of frames.

2.2 Image Processing Procedures

The image processing method developed in TS consists of 7 sequential processing steps. Detailed description of the developed image processing method and the basic conditions, criteria, difficulties, and limitations of the image processing will be published in our recent publication [12].

a) RGB (Red Green Blue) to gray scale conversion.

Most CCD cameras used for fusion plasma observation record either RGB in the visible range or gray scale intensity information in Visible-IR range. Since visible CCD arrays have different sensitivity and calibration factors for each wavelength in the range of the observation, a complex calibration procedure has to be performed for every wavelength of interest prior to record RGB images. Therefore, to avoid such calibration problem while maintaining intensity information, TS RGB images are converted to gray scale images using a standard conversion equation. Figure 1 a) shows a target TS image converted into gray scale. In the case of AUG, CCD images are recorded as gray scale images.

b) Apply filters to eliminate noise.

Logical filters can be used to enhance specific information or remove noise in the target frame and background frame. The gray scale images are processed by two sequential noise reduction filters.

c) Background subtraction.

Background subtraction is performed to remove the plasma background emission, hot spots, and visible in-vessel structures from the image. Figure 1 b) is a defined background for the process (how to define a background see Ref [12]). Ideal background subtraction would give information only on the dust trajectories. Note that the saturation of the CCD array may cause a “loss of information” for finding the origin of the DCEs during the background subtraction. Nevertheless, the integration (see below and Ref [12] more in detail) of large numbers of frame ensures the location of the origin. Figure 1 c) shows the target frame after the background subtraction.

d) BW conversion to eliminate intensity dependence.

In order to count the “number of DCEs”, trajectories in a frame have to be clearly distinguished by well defined edge (value 1 for trajectories and 0 for background). Thus, the background-subtracted gray scale images are converted to 1 bit black and white (BW) image. Figure 1 d) shows the target frame after the BW conversion of Figure 1 c).

e) Counting number of dust trajectories in frames.

A built in MATLAB® function counts number of contours (area of value 1 surrounded by value 0), total occupied number of pixels (size), and centre of mass, etc. Statistics of the short temporal evolution of the DCEs in a shot as well as a long term temporal evolution in a whole campaign are obtained. Figure 1 e) shows the result obtained by analyzing the target frame Figure 1 d): 1 trajectory is found with the occupied pixel area of 82 pixels.

f) Integration of processed 1 bit frames.

In order to locate spatial position where the most of the DCEs occur, large numbers of frames have to be integrated. In this way, although the information on individual DCE is lost, the overlap of the trajectories indicates the most possible origins of the DCEs in the vacuum vessel. The statistical noise handling and the saturation of pixels on the CCD camera are also considered. As we have described in the beginning of this section, our target pattern in the image processing is straight line-like dust trajectories. Thus, events like MARFEs (multifaceted asymmetric radiation from the edge) and large blobs observed in CCD images are excluded. The final contour plot is obtained.

g) Contour plots and number of DCEs as a function of time.

Contour plots show the spatial distribution of the DCEs (most possible origin) in the vacuum vessel. We define here a variable, Normalized Contour Value (NCV), which represents the number of DCE overlaps divided by total plasma operation time of the integrated shots at each pixel. This is due to the different plasma operation time of different shots: The longer the shot is, the more DCEs may present. Thus, the NCV is the integrated frequency of the DCEs representing the temporal evolution of the trajectories. Figure 2 shows the explanation of the physical meaning of the NCV in the contour plot. Dashed lines represent in-vessel components of TS (see Figure 3). Suppose that ten one-second discharges are performed. In each shot, one DCE is observed and recorded. Integrating processed images and divide contour value (number of DCE overlaps) by total operation time of 10 seconds. If there are places where DCEs are overlapped several times, the NCV at the overlapped location (pixels) will be high (e.g., 0.5 in Figure 2). The more overlap of trajectories is, the higher is the NCVs at the overlapped pixels. On the other hand, if the trajectories in shots are completely random or show less overlap, the contour plot shows a broad distribution of DCEs and the NCVs have low values (e.g., 0.1 in Figure 2) [12]. In such a case, it is hard to identify patterns of spatial location of the DCEs, thus the locations of origins.

Using the final contour plot with NCV, statistics for each in-vessel component such as outboard limiter (OL), toroidal pumped limiter (TPL) and high field side (HFS) inner and low field side (LFS) outer walls were obtained: Additional matrices representing components defined by 0 and 1 - 1 for region of interest (e.g. TPL) and 0 for elsewhere - are multiplied to the final contour plot (as shown in Figure 6) and four contour plots of each component (OL, LFS, HFS, TPL, except for the camera view in Figure 3) are obtained. For an absolute comparison among the components that occupy different pixel areas, the NCVs of each contour plot are divided by total pixel number of each component (antenna: 3496 pixels, HFS wall: 40370 pixels, LFS wall: 32466 pixels, TPL: 10057 pixels) to get the Normalized Contour Value Per Pixel (NCVPP), which is corresponding to both frequency and spatial density of the

NCV: high NCVPP means that DCEs occur more frequently and more localized in the in-vessel component.

3. Results and Discussions

In this section, we report the analyses of DCEs observed during plasma operations in TS and in AUG. Temporal evolutions and spatial distribution of the DCEs of TS CIMES campaign in 2006 [18], DITS (Deuterium Inventory in Tore Supra) campaign in 2007 [19], and AUG campaign in 2007 has been studied in detail. TS and AUG have different configurations - TS is a carbon limiter machine and AUG is a full tungsten divertor machine – and these studies will address the DCEs depending on the machine configuration and wall materials.

The term “short term temporal evolution” means DCEs evolution during a single shot from the start up to the end of the shot (see Figure 4, for instance). Typical plasma operation of a shot in TS is about 10-20 seconds with 2 second ramp up, 8-14 second flat top, and 250 ms – 4 second ramp down, whereas a shot in AUG is shorter than that of TS, about 5-8 seconds with 0.9 second ramp up, 1.5-5.5 second flat top, and 0.6-1.5 second ramp down. The term “long term temporal evolution” means the DCE statistics for a whole campaign. The long term statistics is obtained by integrating short term statistics and is presented as DCEs per second as a function of total plasma operation time (see Figure 5, for instance).

The CCD cameras in TS and AUG have both a frame rate of 25 Hz and image resolutions of 352×288 and 768×576 pixels. The spatial resolution of a pixel is from about 5 mm×5 mm to in front of the cameras to 10 mm×10 mm at a point far from the CCD cameras.

3.1. Dust Creation Events in CIMES Campaign in Tore Supra

The objective of the CIMES project is to provide Tore Supra for pulse lengths up to 1000 s with heating and current drive systems capable of delivering a total power of order 20 MW, and a fuel injection system with necessary reliability and high performance. During the CIMES campaign, plasmas with maximum power coupling of about 10 MW of Ion Cyclotron Resonance Heating (ICRH) and LH (Lower Hybrid resonance heating), B_{tor}=3.7 T, I_p=0.9 MA are performed. More in detail for CIMES project can be found in the reference [18].

3.1.1. Short Term Temporal Evolution

Figure 4 shows the short term temporal evolutions of DCEs at the beginning of the CIMES campaign in 2006. In this period, most of the shots are ohmic (see Figure 5, opened circles). The corresponding plasma operation phase, i.e. current ramp up (dotted line), flat top (solid line), and ramp down (dashed line), is depicted (different color indicates individual shot).

Figure 4 a) shows the short term temporal evolutions of 10 ohmic shots at the very early phase of the campaign after about 100 seconds of plasma operation time. Two groups of heavy flaking events were identified. The first group is just after the plasma start up and in the current ramp up phase. In many cases in this phase, it is observed that the plasma touches the guard protection of OL and the antenna protection. Large numbers of DCEs are observed with a maximum DCE number of around 30. During the current ramp up, DCEs decreases. In flat top phase, huge numbers of DCEs due to the strong interaction between the plasma and TS inner PFCs is observed. It seems that this large amount of DCEs comes from microparticles/flakes created during the maintenance period of the machine: A long vent creates flakes inside the vacuum vessel, because of humidity, maintenance activity, etc. As the total plasma operation time increases [see Figure 4 b), 10 ohmic shots after 300 seconds of total plasma operation time], the DCEs in flat top phase decrease corresponding to a real cleaning of the inner wall by cleaning/conditioning discharges and also plasma-wall interaction. Nevertheless, the behaviour of DCEs at the start up and during the ramp up phase remains the same but with smaller DCE numbers. During the ramp down phase, some of DCEs were also observed.

After about 750 seconds of total plasma operation, it is clearly seen from the Figure 4 c) (also see Figure 5) that the DCEs show lowest numbers comparing with that of earlier shots. The vacuum vessel is clean and well conditioned for further experiments. Again, although DCEs during the flat top and ramp down phase show dramatic decrease of DCEs numbers, DCEs at the start up and ramp up phase show relatively large numbers of DCEs. These observations indicate that during the standard operation when the machine is clean, large numbers of dusts are produced during the start up and ramp up phase in TS plasma operations.

3.1.2. Long Term Temporal Evolution

Figure 5 shows the long term temporal evolution of DCEs during about 15000 seconds of total plasma operation time in the CIMES campaign. The y-axis shows the Number of Events per Second (NEPS) defined as the total number of events in a shot divided by total plasma operation time of the corresponding shot - as a function of total plasma operation time in CIMES campaign. NEPS allows the absolute comparison of DCEs among shots along a campaign: The number of DCEs of different physics programmes or operation scenarios may mislead the results, because of different plasma operation time in a shot. Symbols in Figure 5 represent individual power coupling: Opened circle represents ohmic shots while closed circle means ohmic shots after cleaning discharge for a major disruption. Closed square is depicted for LH, closed diamond shows the ICRH coupling. Closed triangle is used for LH+ICRH, asterisk is depicted for LH+ICRH+ECRH (Electron Cyclotron Resonance Heating). At the beginning of the campaign, as we have seen from the three short term temporal evolutions of NEPS in Figure 4 (plasma operation time is corresponding to the box with dashed-line in Figure 5), huge NEPS due to micro particles/flakes created during the vent/maintenance of the machine was observed. The NEPS decreases exponentially as the plasma operation time

increases. At about 750 seconds of the plasma operation, the NEPS reaches its minimum value of about 0.7. The average NEPS in this conditioning phase is about 18. Note that, various different plasma operation scenarios have been used in TS CIMES campaign. Thus, depending on the experimental/physics programs and wall conditions, the NEPS increases or decreases as the campaign proceeded further. Average value of NEPS depending on the power coupling after the minimum point in CIMES campaign is shown in Table 1. Although average NEPSs are in the range of 3.6-6.5, it seems that the general trend of NEPSs in Figure 5 shows a broadening as a function of plasma operation time. Two bars in Figure 5 indicate the broadening of NEPS during the CIMES campaign. Note that, the NEPSs represent DCE count per second regardless the spatial location (cf., see section 3.1.3).

3.1.3. Spatial Distributions of Dust Creation Events

Spatial distributions of DCEs in CIMES campaign depending on the input power coupling are depicted as contour plots in Figure 6 (64 level between 0 and maximum value). Contour values of each figure are normalized to the total operation time of the corresponding scenarios (e.g., ohmic, ICRH, etc) which allows an absolute comparison among the contour plots in Figure 6 as defined in section 2. Shots analyzed and depicted in Figure 6 are randomly chosen from the CIMES campaign, thus, not all the shots are sequentially performed. Note that, contour values of ICRH [Figure 6 c) and 6 f)] are scaled down to one half of their original values, in order to give a clear comparison with other plots in Figure 6.

Figure 6 a) is an original TS RGB CCD image with guide lines dividing the sections of each in-vessel component for more clear comparison. In general, all contour plots in Figure 6 show broad distributions of NCVs (< 0.005) on the TPL which is due to the random DCEs. Most of DCEs occur at the TPL, bottom of HFS inner wall, and the protections of OL and antenna. The broadest distribution of random DCEs is with ICRH+LH as identified by Figure 6 e). Figure 6 b) shows the spatial distribution of DCEs during 22 ohmic shots after cleaning discharge for major disruptions: Highly localized DCEs on the TPL with a maximum NCV of 0.037. Patterns on the TPL are clear and definite. The DCEs at the HFS wall were relatively smaller than other contours in Figure 6 meaning that the plasma-wall interaction at the HFS was weaker. Together with the frequency of total NCV in ohmic shots in the table 2 (the lowest), DCEs in ohmic shot (after the cleaning discharges) occur less frequently, but highly localized on TPL.

49 discharge shots with ICRH are presented in Figure 6 c). A maximum NCV of 0.064 is observed at the top of the vacuum vessel which is the highest value among the contour plots in Figure 6. Some of slightly localized DCE pattern are seen on the TPL, with a broad distributions of random events on the TPL and at the bottom of the HFS wall. DCEs from the OL and its protection were identified. Table 2 indicates that DCEs in ICRH discharges occur most frequently. These results point out that DCEs in

ICRH discharges are randomly distributed and frequently occur meaning very strong plasma-wall interaction.

37 LH discharge shots in Figure 6 d) show also broad random DCEs with some localized DCEs on the TPL and at the bottom of the HFS wall. Broad distribution of NCVs is similar level as in ICRH discharges indicating that DCEs occur also randomly at many different places in short term scale. The contour plot of DITS campaign in section 3.2. which has performed with LH power coupling shows highly localized DCE pattern on TPL. This comparison denotes that the temporal and spatial evolution of DCEs are not simply dependent on the input power coupling only, but also on the history of the vacuum vessel.

The maximum level of NCVs in contour plot of 96 ICRH+LH shots in Figure 6 e) is the lowest among Figure 6. Note that the NCV of ICRH+LH shots shown in table 2 is lower than that of ICRH or LH discharges. These two facts mean that DCEs in ICRH+LH discharges occur less frequently than in ICRH and LH discharges, and large amount of DCEs occur randomly. Nonetheless, localized DCEs on the TPL, at HFS, and at the protection of OL, on the surface of the OL are observed. Figure 6 e) appears to be a superposition of Figure 6 c) and Figure 6 d), and indeed, addition of Figure 6 c) and Figure 6 d) gives a relatively similar contour plot as Figure 6 e). Nevertheless, care must be taken because the similarity doesn't mean that the plasma-wall interaction in ICRH+LH plasma is due to the linear superposition of ICRH plasma with LH plasma. Since LH and IRCH power are sequentially applied during the plasma operation, e.g., LH power is ramped up, and then ICRH is ramped up while LH power is in flat top (or vice versa). Thus, there were several seconds of plasma operation time in ICRH+LH discharges with only LH or ICRH is turned on. Thus, they may induce the similarity between the ICRH+LH contour plot in Figure 6 e) and the contour from the addition of Figure 6 c) and d).

Figure 6 f) shows the contour plot of 14 shots with ICRH+LH+ECRH. The ECRH in TS is not for plasma heating but a diagnostic for electron temperature. However, the use of the ECRH has changed the spatial distribution of the DCEs, as well as increased the number of DCEs at the bottom of the HFS wall [position of label B in Figure 6 a)] comparing with other contour plots in Figure 6.

Summarizing the results from Figure 6, it is clearly shown that temporal evolution and spatial distribution of DCEs are different and strongly dependent on the power coupling. Nevertheless, long term statistical behaviour of DCEs of each input power coupling as a function of input power level shows no definite DCE pattern as shown in Figure 7. Ohmic power is assumed to be 1 MW. Number of DCEs per second is scattered in a broad range of input power regardless of the level of the power and coupling methods. This suggests that the DCEs are not simply dependent on the input power level or coupling method but strongly dependent on the wall condition and history of the plasma operation.

3.1.4. Statistics of Dust Creation Events

Table 2 shows the summary of statistics of DCEs from each in-vessel components depending on the power coupling in TS CIMES campaign. Overall statistics of TS CIMES campaign indicate that ICRH discharges produce DCEs most frequently (80.05: corresponding to event/s). The frequency decreases with the power coupling of ICRH+LH+ECRH (74.68), LH (72), ICRH+LH (67.81), and then ohmic (55.19) discharges. In all discharges, DCEs occur most frequently at TPL with an average NCV of 29.43, which has an average percentage of about 42.66 %. NCVs at LFS are also high with an average NCV of 21.64 and has an average percentage of about 31.11 %: However, care must be taken. As we have mentioned above, because of the 3D to 2D projection and the perspective of the CCD camera, DCEs from the LFS through the plasma volume and from the edge of the HFS inner wall [see label A in Figure 6 a)] cannot be distinguished. Thus the statistics for the LFS may have relatively larger error-bar than that of other components. Average NCV at the HFS is about 15.41 with a percentage of about 21.31 %, and at the OL is the lowest, 3.47 and with 4.93 %. Table 2 shows also different plasma-wall interaction depending on the power coupling. With ohmic power coupling the plasma-wall interaction at TPL (28.59) is the strongest, LFS (18.35), HFS (5.97), and then OL (2.28). ICRH power coupling shows strong plasma-wall interaction at all in-vessel components, HFS (23.75), TPL (26.40), LFS (24.67), and even OL (5.23) compared with other power couplings. NCVs with LH power coupling indicate that the plasma-wall interaction at TPL (29.86) and LFS (28.75) is strong, about one third at HFS (10.62), and weak interaction at OL (2.77). ICRH+LH coupling shows the strong interaction at TPL (26.72), LFS (20.41), HFS (15.78), and then at OL (4.9). ICRH+LH+ECRH power coupling indicates the most frequent interaction at TPL (35.59) in table 2, at HFS (20.91), LFS (16.02), and then OL (2.16). Detailed analysis on the correlation between plasma parameters and DCEs is beyond the scope of this paper. This would be one of our future work programmes.

3.2. Dust Creation Events during DITS Campaign in Tore Supra

In-vessel tritium inventory is a critical issue for ITER. Maximum number of discharge shot will be limited by the T inventory in vacuum vessel which is set to 350 g by nuclear licensing [5, 6]. Therefore, it is important to investigate the fuel retention in existing tokamaks. In order to clarify how and where the hydrogen-isotopes (deuterium or tritium) are trapped in the TS carbon walls, a dedicated plasma campaign (DITS) has been undertaken during which walls were loaded with deuterium in a controlled discharge scenario [19].

During this DITS plasma special procedure, about 180 “similar” long pulse LH discharges with B_{tor}=3.43 T, I_p=0.61 MA, P_{LH}=1.6-1.9 MW, 120 seconds of flat top were performed. Almost 18000 seconds of plasma discharge in total were performed, which is equivalent to 1 year of ohmic plasma operation. This makes the DITS campaign the most ideal campaign for a systematic study of the behaviour of the long term temporal evolution of DCEs with a fixed plasma operation scenario relying mainly on LH plasma heating. The DITS campaign is divided into two phases: The plasma operation time in the phase 1 was 128 seconds in total with 120 seconds LH flat top. In the phase 2, a plasma

operation scenario with a lower LH input power level, 3 seconds of LH ramp up to an initial level, slower increase of LH power in 30-40 seconds, 30 seconds of LH flat top, and 2 seconds of ramp down is used. The reason for the change of the plasma operation scenario will be explained below. At the beginning of the campaign, wall conditioning was performed. Afterwards, neither wall conditioning nor cleaning discharge was performed during the campaign.

3.2.1. Short Term Temporal Evolution

Figure 8 shows overview of the short term temporal evolution of the number of DCEs obtained from 40 individual shots in two different phases of DITS campaign as a function of plasma operation time: 20 shots for phase 1 (shot number between 39758-39981, labels A and B in Figure 9, 10 shots for each) and 20 for phase 2 (shot number between 39985-40060, label C and D in Figure 9, 10 shots for each) are depicted.

General short term temporal behaviour of the DCEs was identical as we have seen in the CIMES campaign (see section 3.1.1). When the plasma touches the protection of OL and antennas just after the plasma start up and in the current ramp up phase, large numbers of DCEs are observed in both phases 1 and 2. During the current ramp up, DCEs rate decreases. When LH power is turned on and ramping up, the DCEs increase due to the change of the plasma-wall interaction and the SOL. After the plasma is settled in flat top phase, DCEs occur occasionally depending on the vessel history, wall condition, and the strength of the plasma-wall interaction (see below). DCEs were also observed during the ramp down phase.

Long plasma operation with unconditioned wall makes the vacuum vessel “dirty” due to the accumulation of re-deposited layer on top of the TPL. As a consequence, numbers of DCEs in shots increase and occur more frequently in later shots of phase 1 as the total plasma operation time increases [Figure 8 a)]. Finally, the plasma operation scenario had to be changed due to the operational difficulties caused by heavy DCEs and frequent disruptions at the end of the phase 1 [19]. After changing the plasma scenario (phase 2), overall number of DCEs was dramatically decreased at the beginning of the phase 2 [Figure 8 b)]. Although the number of DCEs in early shots of the phase 2 is smaller than that in the later shots of phase 1, DCEs occur more frequently (also compare region in Figure 9 label A with C). As the plasma operation time increases further, and large numbers of DCEs were observed. Afterwards DCEs reach almost the same level as that in the later shots of phase 1 (also compare region in Figure 9 label B with D).

3.2.2. Long Term Temporal Evolution

Figure 9 shows the long term evolution of DCEs during 150 shots of the DITS campaign including disruption shots. y-axis of figure 9 shows the NEPS as defined in section 3.1.2. Closed squares indicate the NEPS of normal shots, while closed circles represent disruption shots. First of all, it is found that the NEPS of normal shots has much lower value than that of disruption shots. Often, heavy

flaking leads to a major disruption. However, care must be taken. The NEPS is by definition the number of events divided by plasma operation time which is corresponding to the frequency of DCEs. It does not represent the strength of the flaking effect to the plasmas. Thus, high NEPS does not mean always disruption or vice versa. In the early shots of phase 1, the NEPS of normal shots starts with a value of 0.16, which ensures the minimum level of NEPS as seen in CIMES campaign (0.7). The NEPS of normal shots increases exponentially to a value of 4.29 at the end of the phase 1, about a factor of 27 in 12000 seconds of plasma operation. Physical processes responsible for the exponential increase of NEPS cannot be simply given. Nevertheless, some of general ideas might be given by using known facts of the plasma-wall interaction. Assuming a constant deposition rate (due to the use of the same plasma operation scenario in DITS campaign), the increase of the thickness of deposited layers at the deposition dominant areas is linear as a function of time. As the thickness of the layers reaches a critical point (depending on the condition and history of the layer) that exceeds the limit of the internal stress, flaking occurs. At the spatial point where the flaking has been occurred, a defect between the re-deposited layer-substrate system (CFC of TPL) is created, which diminishes the adhesion of the co-deposited layer. The defect propagates further as the thickness of the co-deposited layer increases with the increased internal stress level. First consequence of this process is the increase of the number of DCEs. Second, as the defect propagates along the interface between layer and the substrate, much larger flakes are ejected more frequently which can be broken into several pieces immediately after the flaking. Such flaking process is often observed in low temperature DLC (Diamond-Like Carbon) thin film growth using hydrocarbon plasmas [20]. Summarizing these hypotheses, smaller flakes are produced at the beginning of the campaign that may not be observed by CCD cameras. As the plasma operation time increases, much larger and more flakes are ejected, broken into several pieces, and then detected by cameras.

Mean value of NEPS of normal shots in the phase 1 is about 2.21. The NEPS of disruption shots is scattered in a wide range of NEPS from 0.35 to 60 with a mean value of 10.52. No specific time dependency is found.

The NEPS decreased down to a level of 1.25 at the beginning of the phase 2 after changing the plasma operation scenario. The mean NEPS increases to 2.7, slightly higher than that of the phase 1, with a maximum value of 8.76. Nevertheless, NEPS is increasing as a function of plasma operation time with almost the same tendency as in the phase 1, and the deviation of NEPS (bars in Figure 9) in both phases are similar. These indicate that the effect of the plasma wall interaction remains almost the same.

The results reveal that the number of DCEs is strongly correlated with the total operation time of the tokamak plasma, if the same and fixed plasma operation scenario is used. As the plasma operation time increases, it is likely that more and more DCEs occur during the campaign, and finally cause operational difficulties. This is a very important and critical issue for next generation reactor type

fusion devices, because re-deposited layers and dust removal have to be planned and performed regularly for such long pulse operations.

3.2.3. Spatial Distributions of Dust Creation Events

Figure 10 shows normalized contour plots (64 level between 0 and maximum value) of integrated images, over 260000 integrated frames of DITS campaign with solid lines dividing section of each in-vessel components as shown in Figure 6 a) for a guide to the eye. Note that, the plasmas in the DITS campaign were all LH plasmas. The scale of the NCV is smaller than that in Figure 6 d), about 1/2. First of all, a broad distribution of DCEs on the TPL and at the bottom of the HFS inner wall is recognisable due to the random DCEs. On the other hand, highly localized DCE patterns on the TPL were identified at similar positions as seen in Figure 6 d). The pattern is easy to identify due to large numbers of integrated frames. The areas are corresponding to the re-deposition of the eroded material. The DCEs from OL are nearly negligible in DITS campaign. The different behaviour between CIMES and DITS LH discharge is because the LH shots in CIMES campaign were performed among other plasma operation scenarios. Frequent change of the power level and coupling in CIMES campaign from shot to shot causes different effect of plasma-wall interaction. Also cleaning discharges were performed if it was necessary. Therefore, the surface conditions on the TPL and inner walls were different that cause different DCE pattern in CIMES campaign.

3.2.4. Statistics of Dust Creation Events

As we have described above, the DITS campaign is an ideal plasma operation to study in-vessel DCEs. Table 3 shows the statistics of the DITS campaign obtained by analyzing final contour plot in Figure 10. As we have seen in the contour plots in Figure 10, most of DCEs are observed on the TPL, with a frequency of 23.64 and a percentage of 71.21 % during the DITS campaign. The frequency of DCEs is comparable with LH shots in CIMES campaign (29.86) indicating that the plasma-wall interaction at TPL would be similar in both cases. On the HFS inner wall, a frequency of 4.54 (10.62 in CIMES) and a percentage of 13.67 % (14.76 % in CIMES) were observed. At the LFS excluding OL, a frequency of 5.02 (28.75 in CIMES) and about 15.11 % (39.92 % in CIMES) of DCEs were found in these areas, and most of them are concentrated on the edge of the HFS inner wall [see label A in Figure 6 a)]. NCVPPs of DITS and CIMES campaigns show that, although overall NCVPP is a factor of four smaller in DITS (3.84×10^{-4}) than that in CIMES (1.50×10^{-3}), the NCVPP at TPL is almost the same in both cases. This indicates that the DCEs in DITS are highly localized at TPL. NCVPPs at other in-vessel components are smaller in DITS campaign, a factor of 2.4 at HFS, a factor of 6 at LFS.

CCD cameras installed in Tore Supra have limited volume of observation. Thus, it is of interest to extrapolate the results to the entire Tore Supra vacuum vessel. To achieve the extrapolation, correction factors for each component have to be considered.

1. The TPL observed by tangential camera is about 27.8 % of entire TPL.
2. Area of HFS inner wall observed by tangential camera is 1/6 of entire HFS surface.
3. Area of LFS outer wall observed by tangential camera is 1/9 of entire LFS surface.
4. 1 OL and 5 antenna protections (similar function as OL).

Table 4 shows the results of extrapolation using the correction factor with an assumption of toroidal symmetry. The extrapolation indicates that the total count number at TPL is about 54 %, about 17.3 % at HFS inner wall, and about 28.7 % at LFS outer wall. Therefore, it can be concluded that the TPL is major source of the DCEs in DITS campaign, especially from the deposition dominant zones.

3.3. Dust Creation Events during 2007 Campaign in ASDEX Upgrade

ASDEX Upgrade is a midsize divertor tokamak. The plasma facing components consist out of tungsten coated carbon. As the erosion rate of tungsten is low, no layers, which could produce dust particles, are found in the main chamber. Layers are only observed at the inner divertor slits, which are not visible by the cameras used. For the campaign 2007 no boronization was applied as initial conditioning. So the first 100 discharges are needed to reach full plasma performance. AUG has the divertor configuration which is different from the limiter configuration in Tore Supra. Thus the DCEs would be different from that in TS.

3.3.1. Short Term Temporal Evolution

Figure 11 shows the overview of the short term temporal evolution of the number of DCEs counted for 30 individual shots of AUG campaign in 2007 as a function of plasma operation time (different color indicates individual shot, 10 shots for each, labels A, B, and C in Figure 12). Unlikely to the short term evolution of DCEs in TS, it seems that the DCEs in AUG occur randomly with no specific DCE pattern depending on the plasma scenario sequence (start up, ramp up, flat top, ramp down). Huge numbers of DCEs are observed at the beginning of the campaign indicating heavy interaction between plasma and walls due to the microparticles/flakes created during the vent/maintenance time of the machine, as in the case of TS. Since microparticles/flakes created on the walls are removed from the vacuum vessel as the total plasma operation time increases, the DCEs decreases more and more, e.g., after about 1000 seconds of the plasma operation time [Figure 11 b)]. After about 1800 seconds of plasma operation, the number of DCEs reaches its minimum level [Figure 11 c)].

3.3.2. Long Term Temporal Evolution

Figure 12 shows the long term evolution of NEPS during the AUG campaign in 2007. The symbols and colours represent NEPS obtained by using different cameras observing different in-vessel positions. Overall trend of the DCEs shows similar tendency as in the case of the early phase of the CIMES campaign in TS. Large numbers of NEPS were observed due to the microparticles/flakes at

the beginning of the campaign. Just after the vacuum vessel is closed and the wall conditioning is performed, the NEPS increases slightly due to the increase of power input level. NEPS start to decrease exponentially as the plasma operation time increases. At about 1800 seconds of the plasma operation, the NEPS reaches its minimum value (0.5). The NEPS at the end of the campaign remains almost at the minimum value. Average values of NEPS for each camera are 19.97 (closed square), 15.41 (closed circle), and 5.68 (closed diamond) events per second. The NEPS in TS CIMES campaign from the beginning of the campaign to the minimum DCE level was 18 (see above), which is very similar to that obtained from the AUG observations. The deviation of NEPS in AUG campaign is small and does not vary much as a function of plasma operation time (bars in Figure 12) even though various plasma operation scenarios have been used. This may come from the divertor configuration, at which the most of DCEs occur in the later phase of AUG operation (see below).

3.3.3. Spatial Distributions of Dust Creation Events

Figure 13 shows the spatial distribution of DCEs in AUG. Figure 13 a) was obtained by integrating 30 shots at the beginning of the campaign in 2007 (Figure 12, label A). The power coupling was mainly ohmic with neutral beam injection (NBI), and additionally ICRH and ECRH. Heavy DCEs are observed from large areas in the machine at the beginning of the campaign as shown in Figure 12 a), especially from the upper part of the machine, side protection, HFS wall, and divertor. NCV shows a maximum number of about 0.57. After about 1800 seconds of plasma operation time, the number of DCEs reaches its minimum. Corresponding contour plot in Figure 13 b) shows that the NCVs are concentrated mainly on the divertor region with a maximum contour value of 0.24 which is factor two lower than that in the beginning [Figure 12 b), integration of 18 shots, see also Figure 12, label C]. Note that, the maximum of NCVs in AUG contour plots are about a factor of ten higher than that in TS. Compare the long term temporal evolutions in Figure 5 and 9 with Figure 12, the numbers of DCEs per second have almost the same order of magnitude. Therefore, higher values of NCVs in AUG mean more localized DCEs and thus more overlaps.

4. Summary and Conclusion

Dust may cause significant problems in ITER. Thus, it is important to understand behaviours of in-vessel dusts during the plasma operation depending on power coupling and machine configuration. During the initial operation phase in a campaign, about 15-20 (average) NEPSs were observed which does not depend on the machine configuration. Proper wall conditioning reduces the DCEs from the vacuum vessel to a level less than 5 NEPS, and then DCEs stays at a lower level. From the short term temporal evolution of DCEs in TS, it is observed that plasma-wall interaction at the plasma start up phase and disruptions generate a large amount of dusts in the case of TS, whereas DCEs have no specific pattern or dependency on the sequence of the plasma operation scenario in AUG.

Contour plots indicate localized origins of the DCEs in both Machines. Most of DCEs occur on the TPL and at the protection of OL in TS with limiter configuration, whereas many DCEs were observed mainly in the divertor region in AUG with divertor configuration. From the TS CIMES campaign, it is shown that the spatial distributions of origins of DCEs are strongly dependent on the power coupling and plasma scenarios, but DCEs occur mainly at the divertor in AUG.

An important message from the DITS campaign is that a fixed plasma operation scenario without wall conditioning results exponential increase of DCEs during the operation and finally causes operational difficulties due to frequent DCEs and disruptions. Highly localized origins of DCEs were observed at deposition dominant zones on the TPL, which indicates the importance of erosion/deposition measurements in existing tokamaks. In order to control DCEs, amount of eroded/re-deposited carbon has to be traced carefully. Concerning this problem, AUG results show that the divertor configuration with full tungsten wall may reduce DCEs significantly during the plasma operation with small deviation as a function of operation time. Nevertheless, due to high divertor heat load in ITER can lead to the melting of tungsten PFC surface which can cause significant amount of dust production. Thus surface melting has to be avoided to keep the dust production low.

Acknowledgement

This work, supported by the European Communities under the contract of Association between EURATOM and CEA, was carried out within the framework of the European Fusion Development Agreement. The views and opinions expressed herein do not necessarily reflect those of the European Commission.

References

[1] N. Bekris, J.P. Coad, R.-D. Penzhorn, S. Knipe, L. Doerr, R. Rolli, W. Nägele, Journal of Nuclear Materials 337–339 (2005) 659–663

[2] G. Federici et al., Nuclear Fusion, Vol. 41, No. 12R (2001), 1967-2137

[3] J. Winter, Plasma Phys. Control. Fusion **40** (1998) 1201–1210

[4] S. Rosanvallon, F. Onofri, P. Delaporte, CFP/NTT-2007.030, "Assessment of in-vessel dust measurement and removal techniques for ITER", TW6-TSS-SEA5.1 Delivrable 5 - Final Report

[5] "Generic Site Safety Report – Volume III – Radiological and Energy source terms – July 2004", G 84 RI 3 R0.2.

[6] "Generic Site Safety Report – Volume VIII – Ultimate safety margins – July 2004", G 84 RI 7 R0.2.

[7] W. P. West et al., Plasma Phys. Control. Fusion 48 (2006) 1661

[8] R. D. Smirnov et al, Phys. Plasma 14 (2007) 112507

[9] K. Sasaki et al, Journal of Nuclear Materials, Vol. 363-365, (2007) P238-241

[10] D.L. Rudakov et al, Journal of Nuclear Materials, Vol. 363-365, (2007), P227-232

[11] M. Rubel et al, Nuclear Fusion, Vol. 41, No. 8, 1087-1099

[12] S.-H. Hong, C. Grisolia, P. M. –Garbet, Plasma Phys. Control. Fusion 51 (2009) 075013

[13] A. Ekadahl et al, J. Nucl. Mater.390-391 (2009) 806-809

[14] R. D. Smirnov et al, Plasma Phys. Control. Fusion 49 (2007) 347-371

[15] J. H. Yu et al, J. Nucl. Mater. 390-391 (2009) 216-219

[16] Ph. Chappuis et al, J. Nucl. Mater. 290-293 (2001) 245-459

[17] J. Phillip Sharpe et al, J. Nucl. Mater. 313-316 (2003) 455-459

[18] B. Beaumont, A. Becoulet, P. Bibet, C. Darbos, P. Garin, A. Géraud, G. Giruzzi, A. Grosman, G. Martin, M. Ottaviani, Y. Peysson, B. Saoutic, P. Stott and M. Zabiego, Fusion Engineering and Design, Volumes 56-57, October 2001, Pages 667-672

[19] B. Pegourie et al., "Overview of the Deuterium Inventory campaign in Tore Supra:operational conditions and particle balance", 18th International Conference on Plasma Surface Interactions (2008)

[20] S. Hong, Ph.D. Thesis, "From Thin Films to Nanoparticles: Investigation of Polymerization Processes in Capacitively Coupled Hydrocarbon Plasmas", Ruhr-University Bochum, Bochum, Germany, (2004)

Figure Captions

Figure 1. The sequence of image processing. a) target TS image converted into gray scale, b) defined background, c) target frame after the background subtraction, d) target frame after the BW conversion, e) result obtained by analyzing the target frame.

Figure 2. Explanation of the physical meaning of the NCV in the contour plot.

Figure 3. The definition of matrices for each in-vessel components used for the individual statistics for K1 camera in Tore Supra.

Figure. 4. Short term temporal evolutions of DCEs at the beginning of the CIMES campaign in 2006 (dashed box in Figure 3). Corresponding plasma operation scenario, i.e. current ramp up (dotted line), flat top (solid line), and ramp down (dashed line), is shown.

Figure. 5. Long term temporal evolution of DCEs during the whole CIMES campaign. Y-axis indicates the number of events per second (NEPS)

Figure. 6. Spatial distributions of DCEs in CIMES campaign depending on the input power coupling. a) original RGB image of Tore Supra, b) Ohmic, c) ICRH, d) LH, e) ICRH+LH, f) ICRH+LH+ECRH.

Figure. 7. Overview of DCEs depending on input power level and coupling methods. Symbols represent ohmic (open circles), LH (closed squares), ICRH (closed diamonds), ICRH+LH (closed triangles), and ICRH+LH+ECRH (asterisks).

Figure. 8. Overview of short term temporal evolution of the number of DCEs obtained from 40 individual shots in two different phases of DITS campaign as a function of plasma operation time (different color indicates individual shot): 20 shots for phase 1 (shot number between 39758-39981, labels A and B in Figure 6, 10 shots for each) and 20 for phase 2 (shot number between 39985-40060, label C and D in Figure 6).

Figure. 9. Long term evolution of DCEs during the DITS campaign including disruption shots.

Figure. 10. Contour plots of integrated images, over 260000 integrated frames of DITS campaign with solid lines dividing section of each in-vessel components as shown in Figure 6 a).

Figure. 11. Overview of the short term temporal evolution of the number of DCEs counted from about 30 individual shots of AUG campaign in 2007 as a function of plasma operation time (different color indicates individual shot, 10 shots for each, labels A, B, and C in Figure 12).

Figure. 12. Long term evolution of DCEs during the AUG campaign in 2007. The symbols and colours represent NEPS obtained by using different cameras observing different in-vessel positions.

Figure. 13. Spatial distribution of DCEs in AUG. a) obtained by integrating 30 shots of the campaign in 2007, see Figure 12, label A, b) obtained by integrating 18 shots, see also Figure 12, label C.

Power Coupling	Average NEPS
Ohmic	6.54
Ohmic after cleaning discharges for major disruptions	5
LH	3.655
ICRH	6.228
LH+ICRH	5.295
LH+ICRH+ECRH	4.733

Table 1. Average NEPS depending on power coupling in TS CIMES campaign.

Location	Power Coupling	Sum of Contour Value (raw data)	Normalized Contour Value (frequency)	Normalized Contour Value per Pixel (spatial density per second)	%
Outboard Limiter	**Ohmic**	684	2.28	6.52×10^{-4}	4.13
	ICRH	4404	5.23	1.50×10^{-3}	6.54
	LH	1847	2.77	7.91×10^{-4}	3.84
	ICRH+LH	9686	4.9	1.40×10^{-3}	7.23
	ICRH+LH+ECRH	657	2.16	6.18×10^{-4}	2.89
	Average	3456	3.47	9.922×10^{-4}	4.93
HFS inner Wall	**Ohmic**	1791	5.97	1.48×10^{-4}	10.82
	ICRH	19987	23.75	5.88×10^{-4}	29.67
	LH	7094	10.62	2.63×10^{-4}	14.76
	ICRH+LH	31201	15.78	3.91×10^{-4}	23.28
	ICRH+LH+ECRH	6356	20.91	5.18×10^{-4}	28.00
	Average	13286	15.41	3.82×10^{-4}	21.31
TPL	**Ohmic**	8574	28.59	2.84×10^{-3}	51.80
	ICRH	22215	26.40	2.60×10^{-3}	32.98
	LH	19941	29.86	3.00×10^{-3}	41.48
	ICRH+LH	52811	26.72	2.70×10^{-3}	39.40
	ICRH+LH+ECRH	10820	35.59	3.50×10^{-3}	47.66
	Average	22872	29.43	2.93×10^{-3}	42.66
LFS	**Ohmic**	5502	18.35	6.02×10^{-4}	33.24
	ICRH	20762	24.67	8.10×10^{-4}	30.82
	LH	19194	28.75	9.44×10^{-4}	39.92
	ICRH+LH	40353	20.41	6.70×10^{-4}	30.10
	ICRH+LH+ECRH	4870	16.02	5.26×10^{-4}	21.45
	Average	18136	21.64	7.10×10^{-4}	31.11
Total	**Ohmic**	16551	55.19	3.84×10^{-4}	100
	ICRH	67368	80.05	1.20×10^{-3}	100
	LH	48076	72.00	1.50×10^{-3}	100
	ICRH+LH	134051	67.81	5.06×10^{-4}	100
	ICRH+LH+ECRH	22705	74.68	3.30×10^{-3}	100
	Average	49096	69.95	1.38×10^{-3}	100

Table 2. Statistics of DCEs from in-vessel components in TS CIMES campaign.

Location		Sum of Contour Value (raw data)	Normalized Contour Value (frequency)	Normalized Contour Value per Pixel (spatial density per second)	%
K1 Camera	**Outboard Limiter**	21	1.67×10^{-3}	4.78×10^{-7}	5×10^{-5}
	HFS inner Wall	57353	4.54	1.12×10^{-4}	13.67
	TPL	298754	23.64	2.35×10^{-3}	71.20
	LFS	63391	5.02	1.55×10^{-4}	15.12
	Total	419519	33.20	3.84×10^{-4}	100

Table 3. Statistics of DCEs from in-vessel components in TS DITS campaign.

Location		Sum of Contour Value (raw data)	Factor	Sum of Contour Value (extrapolation)	%
K1 Camera	**Outboard Limiter**	21	6	126	0
	HFS inner Wall	57353	6	344118	17.3
	TPL	298754	3.6	1075514	54
	LFS	63391	9	570519	28.7
	Total	419519	-	1990277	100

Table 4. Extrapolation of statistics of DCEs from in-vessel components based on TS DITS campaign.

a)

b)

c)

d)

e)

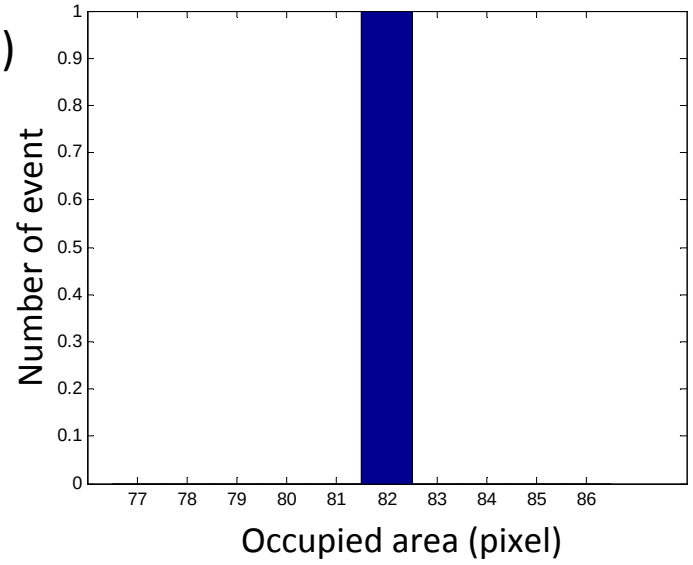
Number of event
0
0.1
0.2
0.3
0.4
0.5
0.6
0.7
0.8
0.9
1
77
78
79
80
81
82
83
84
85
86
Occupied area (pixel)

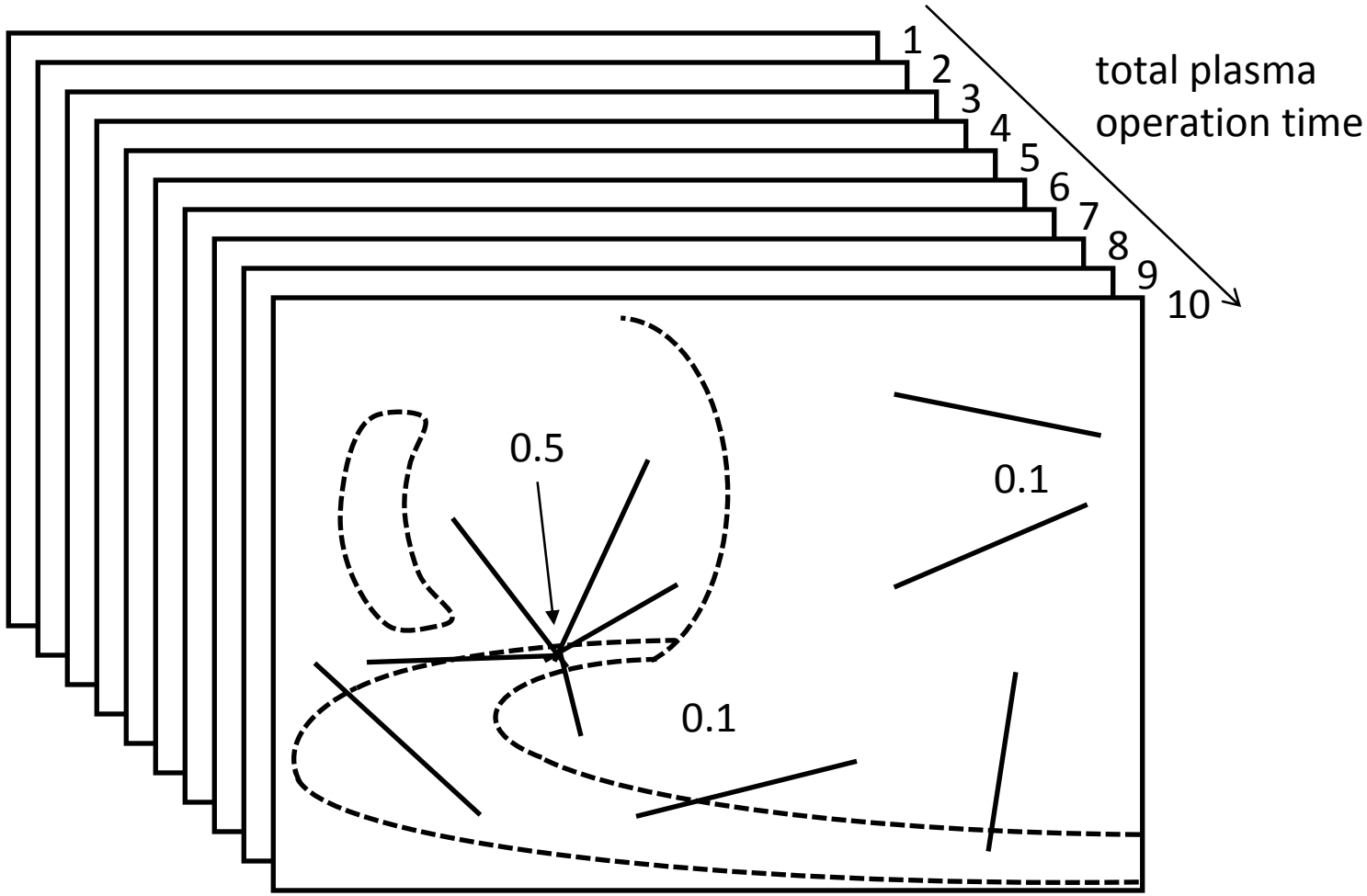

Figure 2

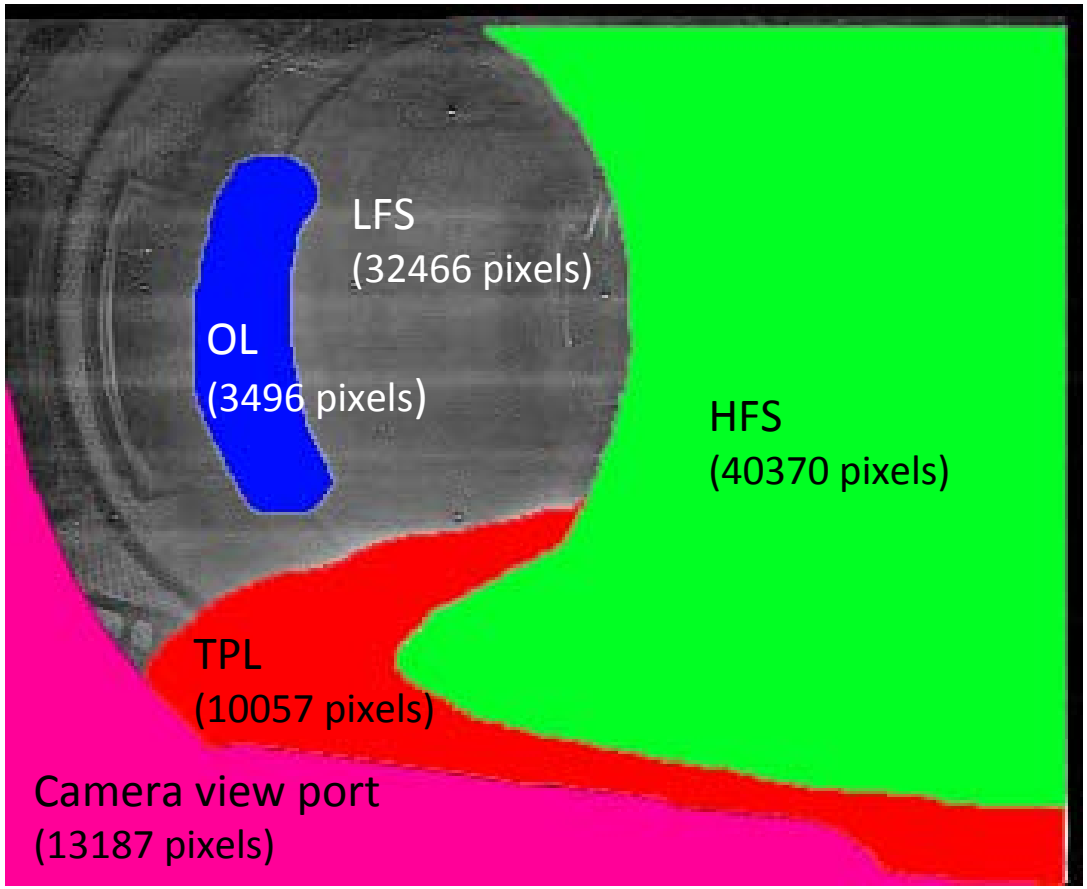
LFS
(32466 pixels)
OL
(3496 pixels)
HFS
(40370 pixels)
TPL
(10057 pixels)
Camera view port
(13187 pixels)

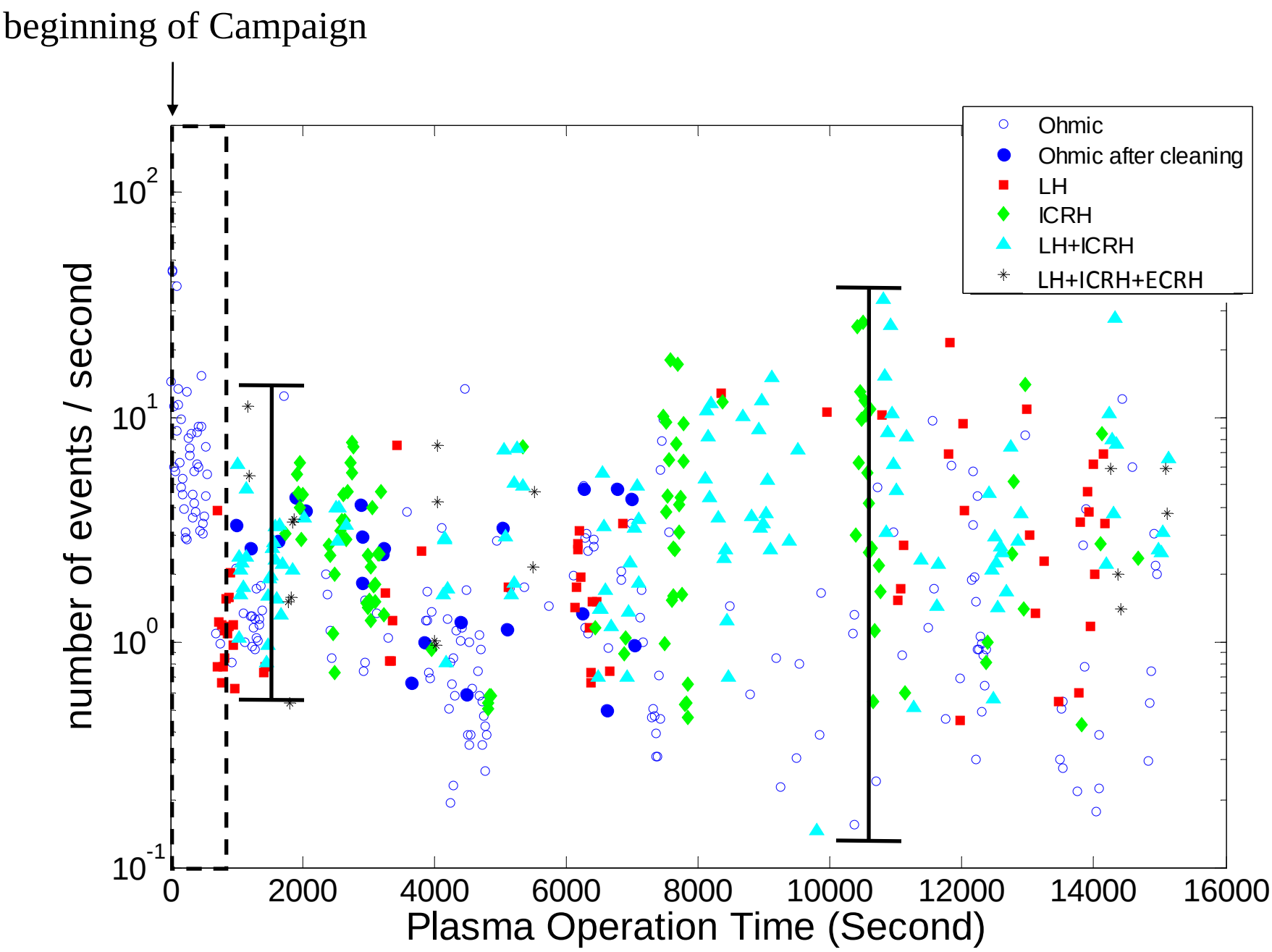

Figure 5 Long term temporal... S. Hong et al

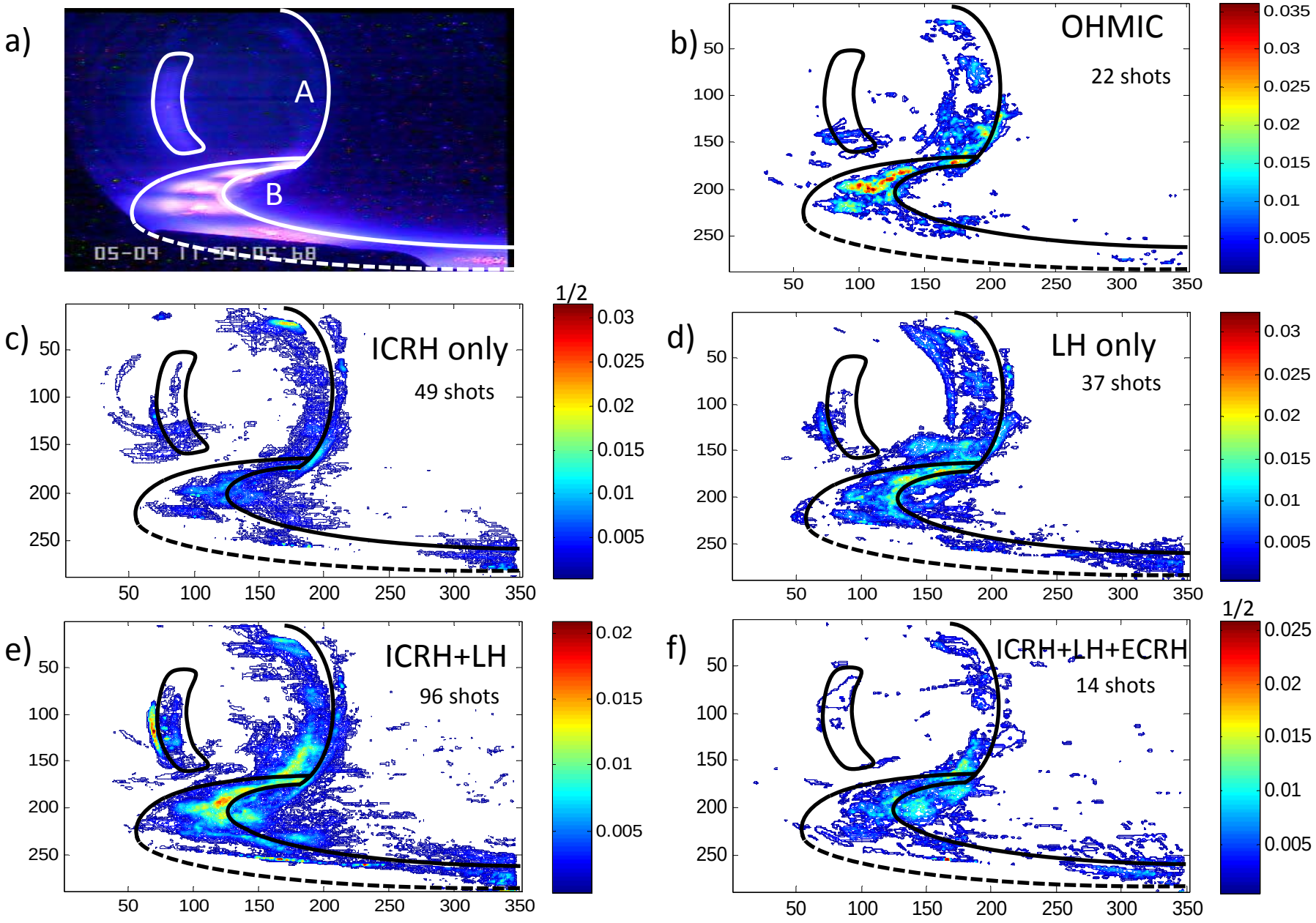

Figure 6 Long term temporal... S. Hong et al

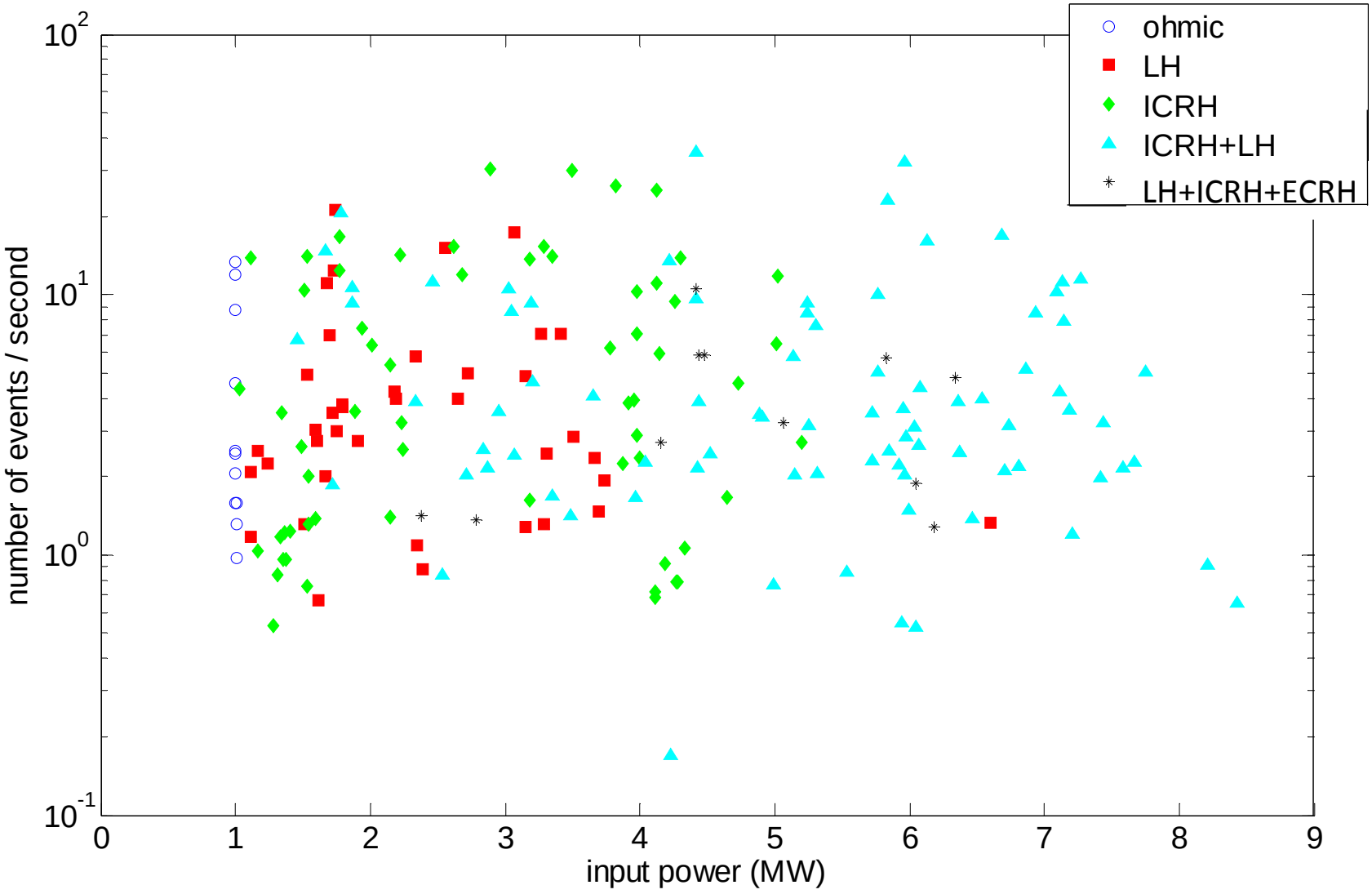

Figure 7 Long term temporal... S. Hong et al

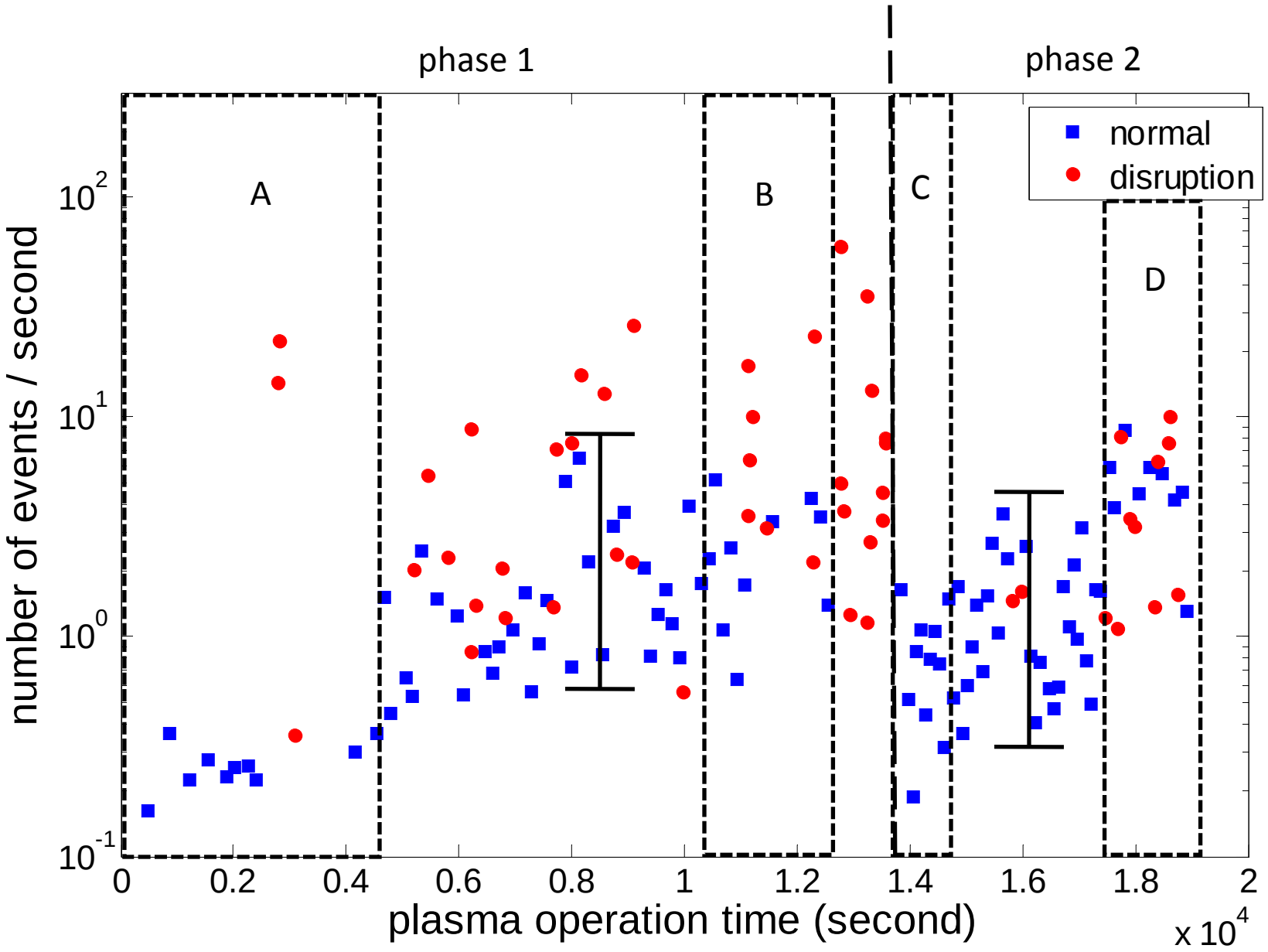

Figure 9 Long term temporal... S. Hong et al

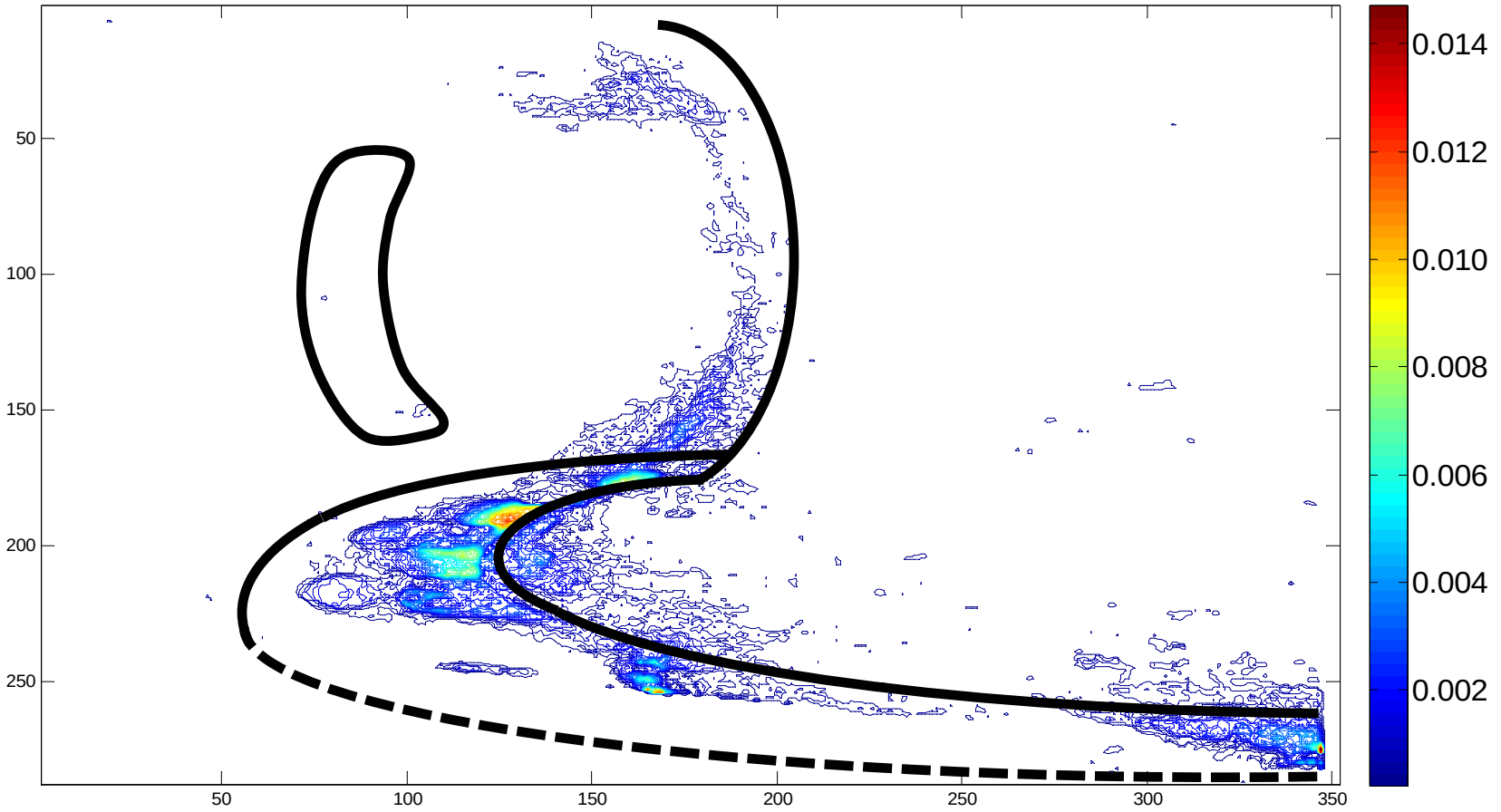

Figure 10 Long term temporal... S. Hong et al

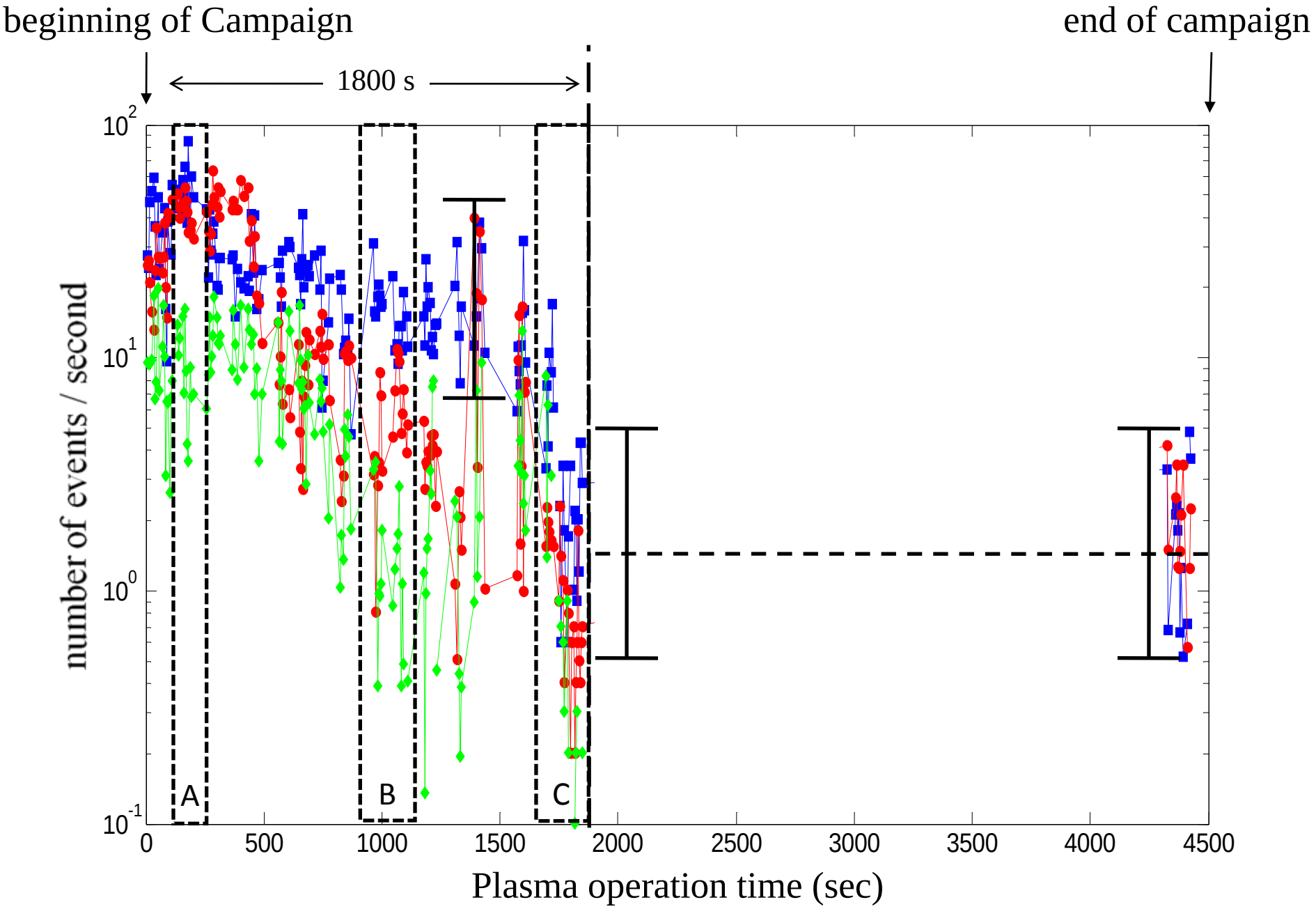

Figure 12 Long term temporal... S. Hong et al

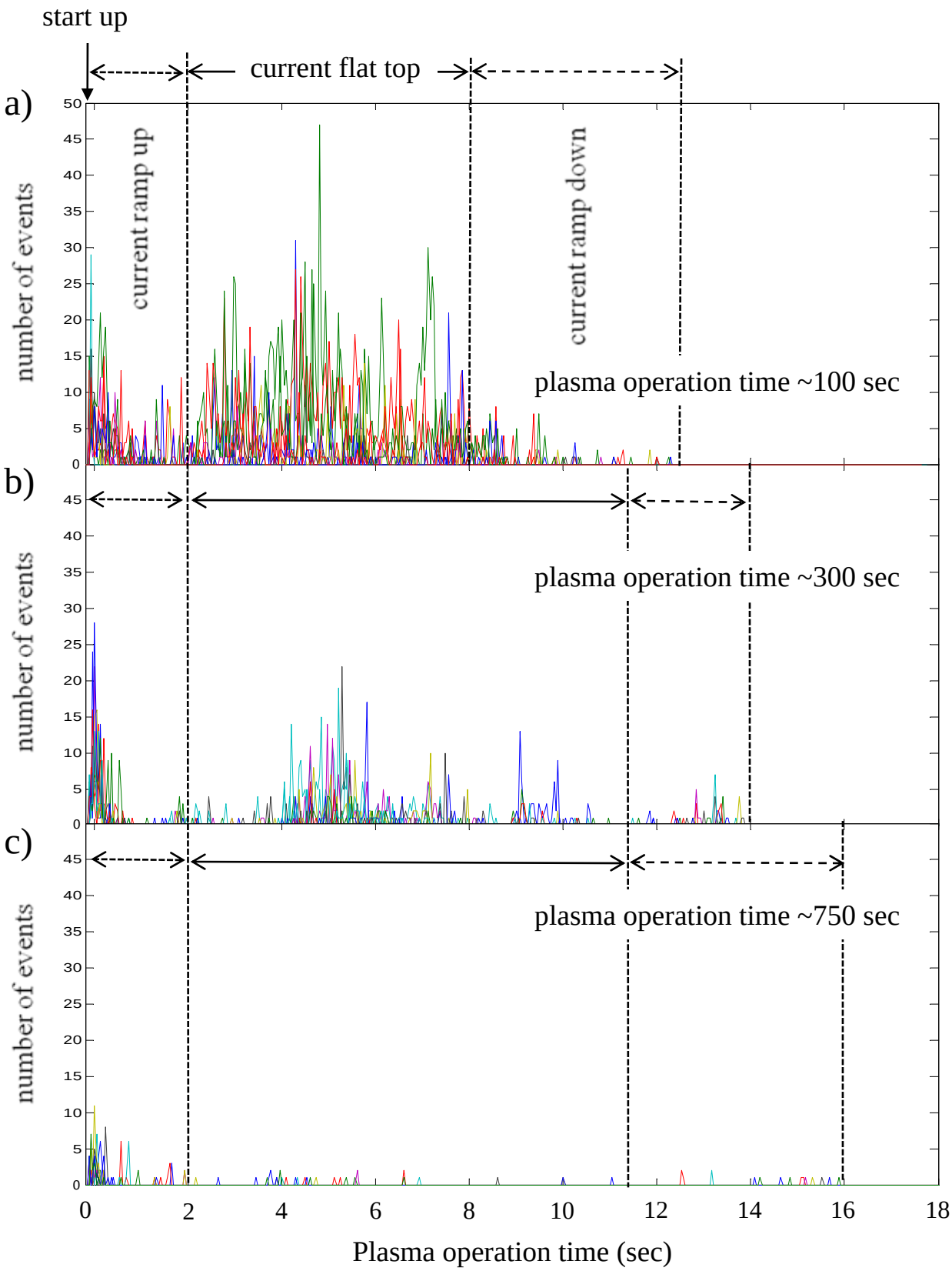

Figure 4 Long term temporal... S. Hong et al

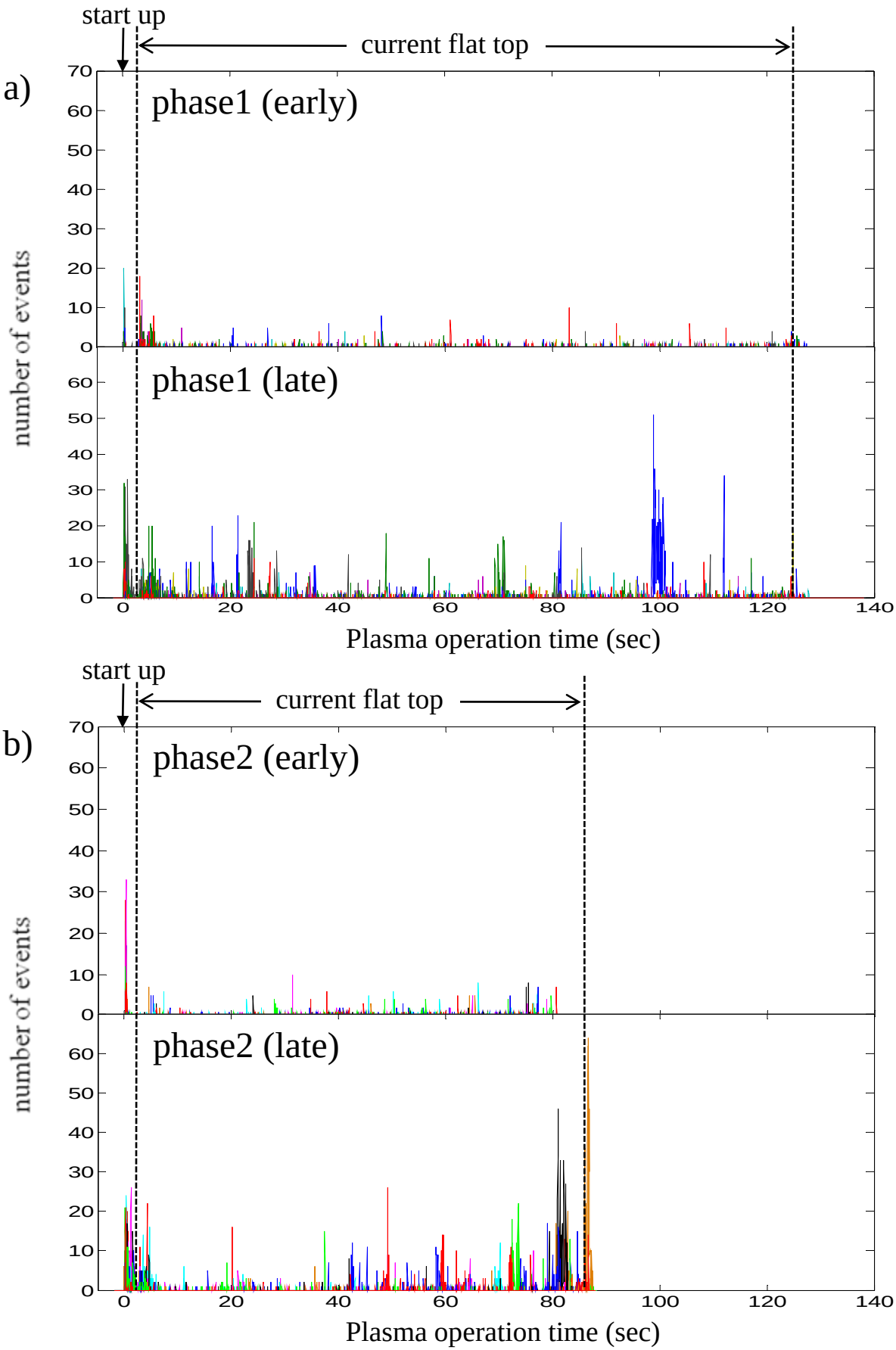

Figure 8 Long term temporal... S. Hong et al

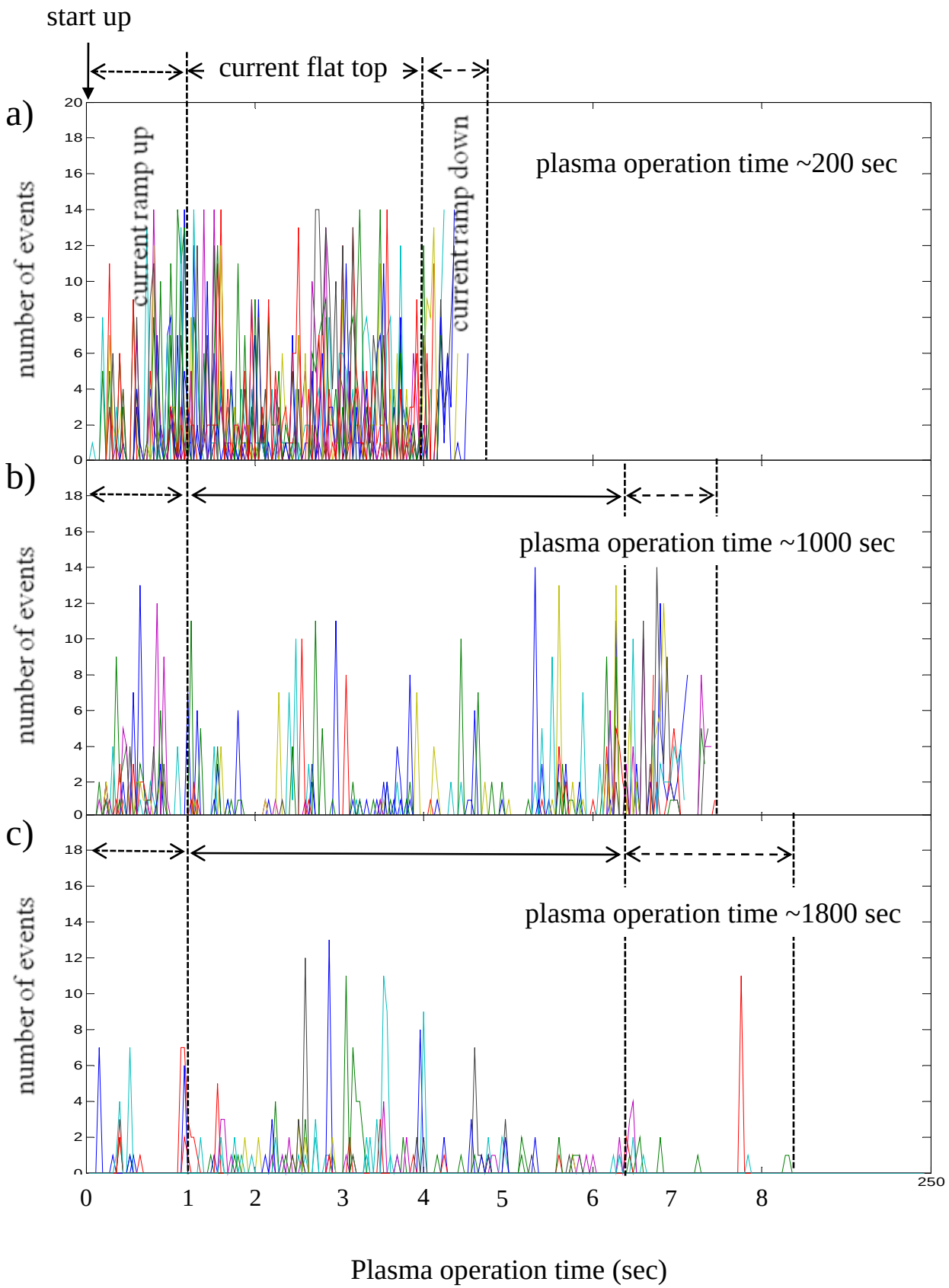

Figure 11 Long term temporal... S. Hong et al

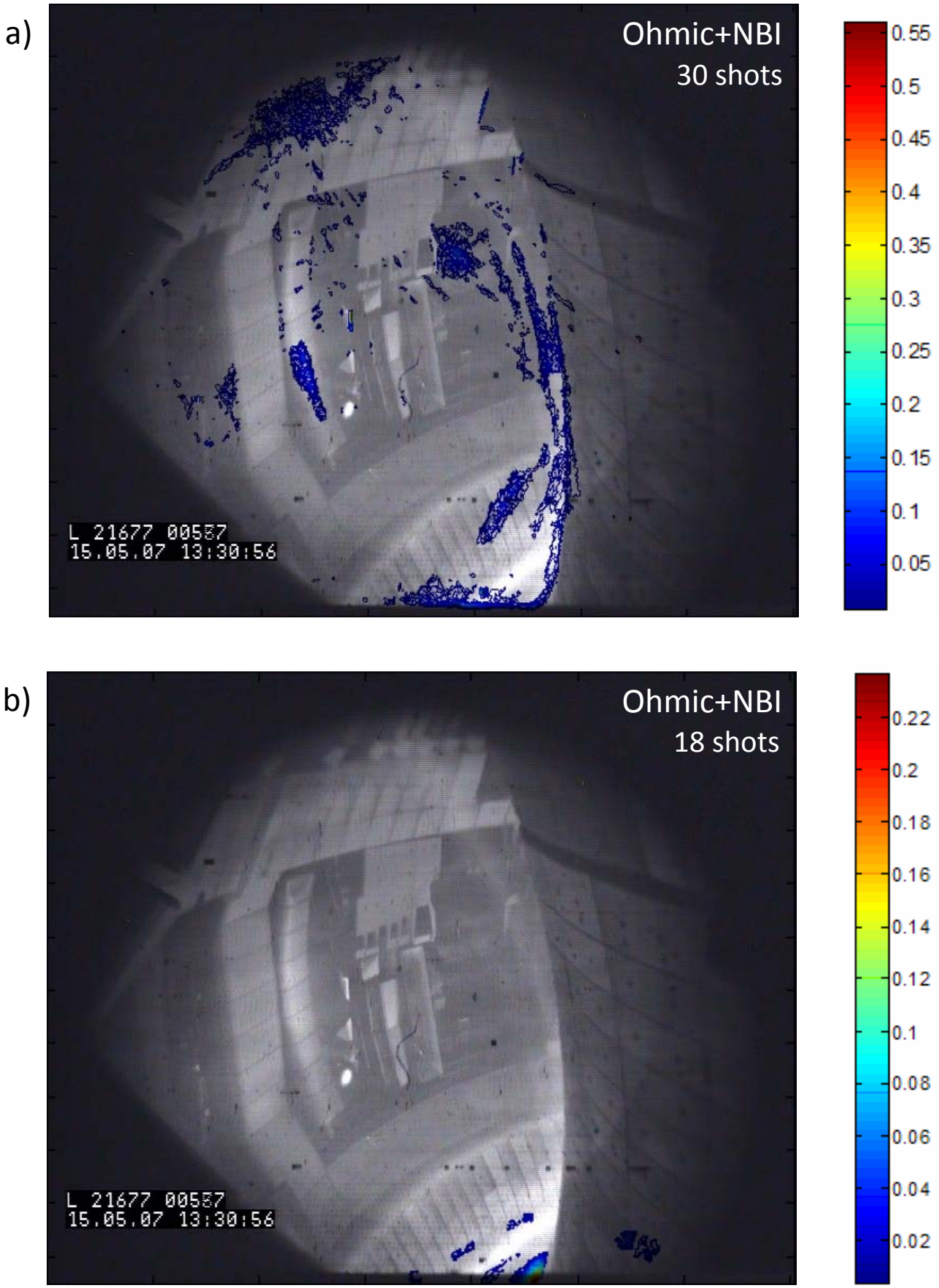
a)
Ohmic+NBI
30 shots
L 21677 00587
15.05.07 13:30:56
0.55
0.5
0.45
0.4
0.35
0.3
0.25
0.2
0.15
0.1
0.05
b)
Ohmic+NBI
18 shots
L 21677 00587
15.05.07 13:30:56
0.22
0.2
0.18
0.16
0.14
0.12
0.1
0.08
0.06
0.04
0.02